Received: 25 May 2020 | Revised: 5 January 2021 | Accepted: 31 January 2021 | Published on: 9 March 2021

DOI: 10.1002/qj.3995

Quarterly Journal of the Royal Meteorological Society RMetS

RESEARCH ARTICLE

Weak cooling of the troposphere by tropical islands in simulations of the radiative-convective equilibrium

David Leutwyler | **Cathy Hohenegger**

Max Planck Institute for Meteorology, Hamburg, Germany

Correspondence
D. Leutwyler, Max Planck Institute for Meteorology, Hamburg 20146, Germany.
Email: david.leutwlyer@mpimet.mpg.de

Funding information
Swiss National Science Foundation, Grant/Award Number: P2EZP2_178503

Abstract

We assess whether tropical islands tend to warm or cool the troposphere. To this end, we use idealized simulations of the radiative-convective equilibrium employing a simulation domain that contains flat tropical islands represented by a land surface scheme. Results show more frequent precipitation over land as coastal breezes establish, and gravity waves triggered by afternoon convection propagating away from the islands. These waves horizontally homogenize density and in doing so communicate convectively induced temperature anomalies from the islands onto the ocean. What is the influence of the islands on tropospheric temperature? The diurnal surface warming of the islands tends to push the afternoon convection over land towards a warmer moist adiabat and, along with it, the temperature profile of the troposphere. However, at the same time, drying of the land surface pulls it towards a colder moist adiabat. All in all, we find that islands cool rather than warm the troposphere. More specifically, we obtain a weakly colder domain-mean troposphere during episodes with a larger share of precipitation over land, or when the prescribed land fraction is increased. In particular, we find that the cooling becomes more pronounced over large islands. Overall, the results indicate that the inability of evaporation to keep up with the daytime surface warming over land, in contrast to the ocean, is of key relevance for understanding land effects on the mean climate.

KEYWORDS

convection-resolving models, deep convection, gravity wave, land–atmosphere interaction, lifting condensation level, moist adiabat, tropical island

1 | INTRODUCTION

Rainfall in the Maritime Continent is strongly shaped by islands and mostly originates from daily thunderstorms (e.g., Yamanaka *et al.*, 2018). The islands act as surface heterogeneities that drive diurnal thermally induced mesoscale circulations in response to the variations in surface fluxes (Segal and Arritt, 1992; Avissar and Liu, 1996). The forcing provided by the circulations facilitates frequent initiation of clouds which then convect into a (neutrally stable) atmosphere following a moist adiabatic lapse rate (Betts, 1982; Xu and Emanuel, 1989). Once

mature and precipitating, the clouds further enhance rainfall over and next to the islands (Sobel *et al.*, 2011; Wang and Sobel, 2017; Ruppert and Chen, 2020); and sometimes they organize into Mesoscale Convective Systems (Houze *et al.*, 1981; Mori *et al.*, 2004) or excite offshore-propagating gravity waves (Mapes and Houze, 1993; Love *et al.*, 2011; Coppin and Bellon, 2019; Ruppert and Zhang, 2019). Factors controlling the spatial distribution and amount of precipitation over islands, in particular interactions between convection and sea breezes, have been studied extensively (e.g., Yang and Slingo, 2001; Qian, 2008; Robinson *et al.*, 2008; Cronin *et al.*, 2015; Ulrich and Bellon, 2019). The effects of islands on the mean tropical climate has so far received less attention. Here we aim at addressing the question of whether islands tend to warm or cool the tropical troposphere beyond their immediate outline.

The mechanism providing the means for local temperature perturbations to project onto the regional environment is that of horizontal density adjustments. In the deep Tropics, horizontal density anomalies occurring in the mid-troposphere are eliminated by gravity waves (Bretherton and Smolarkiewicz, 1989). These rapidly spreading waves induce subsidence that warms the environment of the convective clouds, and in this way tie the large-scale (density) temperature profile of the troposphere to the moist adiabat set by the deep convective clouds. In other words, the troposphere needs to adjust to the characteristic temperature of its clouds since it cannot sustain the density anomalies they induce. This theory is fundamental to the tropical atmosphere and is commonly referred to as the weak temperature gradient approximation (Sobel *et al.*, 2001); or the weak buoyancy gradient, or the weak density gradient approximation (Yang, 2018). However, what adiabat is the troposphere ultimately tied to? More specifically, can the presence of land shift that profile to higher or lower temperatures? For that to happen, the clouds associated with islands need to be different from those originating over the ocean. We argue that the near-surface temperature and humidity anomalies induced by the islands provides the prerequisite for them to become so.

In idealized simulations of the radiative-convective equilibrium (RCE), Cronin *et al.* (2015) found that the presence of islands tends to warm the troposphere. They conducted RCE simulations that included one circular island surrounded by ocean. Overall, they found that the island led to a warming that exceeded 1 K, once the land fraction covered more than 10% of the computational domain. The warming was attributed to the distinct timing of cloud fraction between land and ocean (cloud radiative effect) and to the warmer sub-cloud layer over land. The latter effect is based on the idea that deep convection is usually initiated over the areas exhibiting the highest percentiles of sub-cloud layer equivalent potential temperature (e.g., Emanuel *et al.*, 1994). Cronin *et al.* (2015) argued that the presence of an island inflates the variability of the sub-cloud layer and thus also the tail of the equivalent potential temperature distribution. In other words, deep convection is typically associated with the spatially warmest and moistest near-surface air, and thus deep convective clouds end up on a warmer moist adiabat since, during the day, surface air over the island is warmer than over the ocean. Ultimately, the warmer adiabat is then radiated to the rest of the domain by gravity waves, leading to a comparatively warmer domain-mean temperature profile (also Shamekh *et al.*, 2020).

In the simulations of Cronin *et al.* (2015), the island was represented by an anomaly in the heat capacity of a slab ocean while the parameters entering the surface flux computation maintained oceanic values. While this configuration is elegant, it means that evaporation is never limited by moisture availability, and thus always occurs at its potential rate. We argue that the drying of the soil should be considered as well since this limits evaporation and, through this, affects the temperature profile over the islands. Drying thus moves the atmosphere onto a colder moist adiabat, whereas warming moves it to a warmer moist adiabat. As the soil dries, the near-surface atmosphere will both dry and warm, and it is unclear which one of the two effects wins. In this study, we extend the work of Cronin *et al.* (2015) by considering that evaporation over land can become limited by the available soil moisture, and determine whether islands cool or warm the troposphere in this situation.

We extend the horizontally homogenous non-rotating RCE simulation configuration by including a set of islands. Land surface effects are taken into account using a land surface scheme as commonly employed in weather and climate models. The standard RCE configuration provides a popular configuration for numerical simulation since it depicts a simple model of the tropical atmosphere, which is governed by the balance between warming by convection and cooling by radiation (e.g., Held *et al.*, 1993; Tompkins and Craig, 1998; Bretherton *et al.*, 2005; Wing *et al.*, 2017). Despite the homogeneous initial and boundary conditions, these simulations exhibit feedbacks between radiation, water vapour and deep convection that lead to the self-aggregation of deep convection into large clusters and to the formation and maintenance of distinct dry and moist regions.

It is known that, in the RCE configuration, heteroegenities in the ocean and land surface exert control on the organization of convection. For instance, when anomalies in sea surface temperature (SST) are prescribed, ascending motion and deep convection are commonly found over the highest SSTs and large clusters of convection

slowly migrate towards them (Grabowski *et al.*, 2000; Sobel *et al.*, 2001; Tompkins, 2001; Grabowski, 2006; Shamekh *et al.*, 2020). When an interactive land-surface scheme is employed, the feedbacks become more complicated as shallow circulations triggered by the land surface as well as by the atmosphere compete to set the precipitation distribution (Hohenegger and Stevens, 2018). In particular, Hohenegger and Stevens (2018) made the argument that the ability of the land to dry out was of key relevance to explain the spatial distribution of convection in their idealized land planet.

In the present manuscript, we exploit RCE simulations to further assess the effect of tropical islands on the domain-mean temperature profile. It is structured as follows. The numerical model and the conducted simulations are described in Section 2. The spatial variability of precipitation introduced by breeze circulations over islands, and the communication of convectively induced temperature anomalies from the islands onto the ocean, are illustrated in Section 3.1. Afterward, we assess whether tropical islands tend to warm or cool the domain-mean free tropospheric temperature in RCE simulations using time series analysis (Section 3.2), and simulations containing a smaller land fraction (Section 3.3). In Section 4, we discuss the presented results and formulate a hypothesis explaining why large islands tend to cool the troposphere. Finally, we conclude the study in Section 5.

2 | METHODS

2.1 | Model description

We perform RCE simulations with the fully compressible non-hydrostatic Consortium for Small-scale Modeling model v5.0 (COSMO; Steppeler *et al.*, 2003). It is based on the thermo-hydrodynamical Euler equations, discretized using finite-difference methods on a horizontally regular longitude–latitude–height mesh. The discretization schemes in the dynamical core include a split-explicit three-stage second-order Runge–Kutta time-stepping scheme for the forward integration in time (Wicker and Skamarock, 2002), and a fifth-order upwind scheme for horizontal advection (Baldauf *et al.*, 2011). At the upper model boundary, gravity waves are damped by an implicit Rayleigh damping term acting on the vertical velocity at the end of each acoustic time step (Klemp *et al.*, 2008).

Subgrid-scale processes include an interactive radiative transfer scheme based on the δ-two-stream approach (Ritter and Geleyn, 1992), and a single-moment bulk cloud-microphysics scheme with five hydrometeor species (cloud water, cloud ice, rain, snow, and graupel; Reinhardt and Seifert, 2005). Additionally, subgrid-scale cloudiness is considered in the radiation scheme using a relative humidity-based diagnostic. Besides, the planetary boundary layer is parametrized using an approach based on turbulent kinetic energy (Mellor and Yamada, 1982; Raschendorfer, 2001). Over the islands, the multi-layer soil model TERRA_ML is used. In this soil parametrization, soil water content is predicted using a formulation based on the Richardson equation (Heise *et al.*, 2006). In the current model version, a bedrock formulation is specified at the lowest soil layer, leading to soil water removal by gravitational drainage. The parametrization for convection (shallow and deep) has been switched off.

The presented set of simulations were conducted with a version of COSMO capable of exploiting the capabilities of Graphics Processing Units (GPUs; Fuhrer *et al.*, 2014; Leutwyler *et al.*, 2016). These accelerators appear to be better suited for weather and climate codes than current multi-core processors, mainly because they provide substantial parallelism, higher memory bandwidth, and improved latency hiding (Owens *et al.*, 2008). For the GPU version of COSMO, extensive validation has been conducted using kilometre-scale configurations: It includes a ten-year-long re-analysis-driven simulation over Europe (Leutwyler *et al.*, 2018), validation of clouds (Hentgen *et al.*, 2019), and surface winds (Belušić *et al.*, 2018). Differences between simulations on CPUs and GPUs relate to rounding errors emerging from re-association of mathematical expressions, mathematical approximations or contraction operators, and architecture-specific implementations of transcendental functions (Arteaga *et al.*, 2014; Schär *et al.*, 2020). A first study employing that model version for RCE simulations is presented in Beucler *et al.* (2020).

2.2 | Model configuration and numerical experiments

The present study is based on simulations of the RCE employing fixed SST, no planetary rotation and spatially homogeneous insolation. The configuration follows that of the RCE Model Intercomparison Project (RCE-MIP; Wing *et al.*, 2018), except for using a diurnal cycle of solar insolation with the sun rising at 0600 and setting at 1800 everywhere. The square computational domain ($30° \times 30°$) has been chosen such that a deep gravity wave can horizontally travel the domain within 24 hr, allowing adjustment to density perturbations within one day (Figure 1 in Ruppert and Hohenegger, 2018). Most importantly, the presented simulations contain patches of land, representing flat tropical islands embedded in an ocean with fixed SST (300 K). To obtain a representative island layout, an excerpt

from the Maritime Continent was chosen (10°S–20°N, 104°–134°E). Thereafter all the land overlapping with the domain boundaries was removed, such that the simulation could be run in a double-periodic configuration.

The double-periodic square computational domain contains 1,006 × 1,006 × 74 grid points with a horizontal grid spacing of 3 km, and the time step amounts to 30 s. The vertical direction is discretized using 74 stretched model levels ranging from the first level at 37.5 m to the model top at 33 km. Ten model levels are located below 1 km and Rayleigh damping is applied to the uppermost 30 model levels (i.e., above 18 km height). Soil hydrology is discretized in seven active soil layers that vary from 1 cm thickness at the surface to 2.88 m in the deep soil. The soil type has been set to loam, a common soil type in COSMO simulations (table 11.4 in Doms *et al.*, 2011). Plants are described by a leaf area index of 2.96, a root depth of 2.56 m, and a plant cover of 0.84 (also Schlemmer *et al.*, 2011), and the surface albedo has been set to the same values for land and ocean (0.07). Soil water was initialized fully saturated, and the initial soil temperature was set to the same value as the SST (300 K).

To better understand the control of the land surface on the temperature profile, we conduct simulations for two different island layouts. In the first configuration (10LAND), about 10% of the domain is covered by land. In the second configuration (5LAND), the land fraction was reduced to 5% by removing the island of Borneo. To account for the random nature of convection, simulation ensembles consisting of six 150-day-long simulations were conducted for both island layouts. The different ensemble members were obtained by using a different realization of random noise on the temperature field (0.01 K). The analysis period is defined as the last 50 simulation days (days 100–150).

Note that, although column water vapour reaches a stable value after about 70 days of simulation, the atmospheric moisture budget is not strictly conserved. More specifically, during the analysis phase about 0.021 kg·m^2·day^{-1} of water is unaccounted for, that is, about 1.5% of the latent heat flux is lost. However, we believe that the arguments outlined in the presented article hold nonetheless.

2.3 | Analysis domains

For the analyses presented in Sections 3.1.1 and 3.3, conditional spatial means are computed. The first set of conditions relates to the presence of the islands. Land and ocean are defined by the land mask of the respective simulations (10LAND, 5LAND), and a "Coastal Ocean" region is defined as a L=60 km-wide band (20 grid points) surrounding each island (Figure S1a, b). The width of the band relates to nocturnal land-breezes and the associated precipitation maximum located at L/2 = 30 km off the coast (Section 3.1.1). The second condition is based on the spatial distribution of atmospheric moisture. In traditional simulations of RCE and also in our simulations (also Section 3.1.1), atmospheric moisture horizontally aggregates into coherent wet and dry regions. We define these regions by splitting the domain in half, based on the median of column precipitable water (moist and dry region; Figure S1c). The conjunction of the two sets of conditions defines the Moist/Dry Land, Moist/Dry Ocean, and Moist/Dry Coastal Ocean (Figures S1d–f).

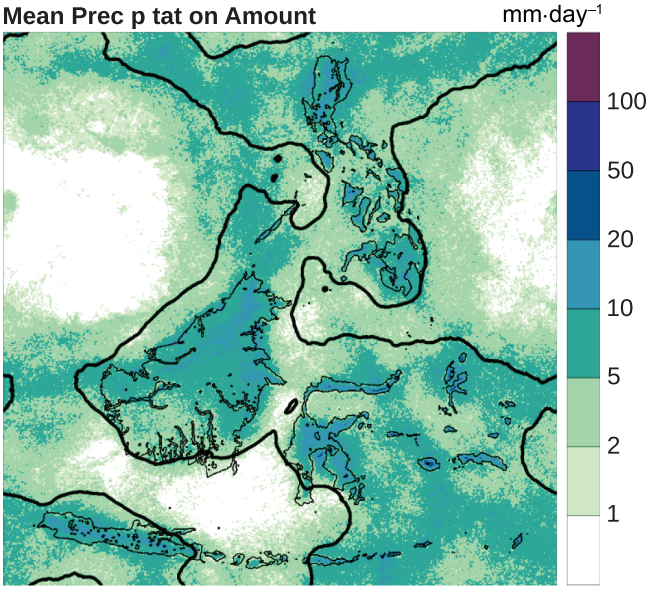

FIGURE 1 Ensemble-mean precipitation amount of the 10LAND simulation averaged for the analysis period (days 100–150). The coloured shading denotes the ensemble-mean precipitation amount and the thin black outlines the prescribed islands. The thick black line marks grid points that correspond to the median value of column precipitable water. It is used to separate the domain into a moist and a dry region. The moist region corresponds to the domain half with more precipitation, and the dry region to that with less [Colour figure can be viewed at wileyonlinelibrary.com]

3 | RESULTS

3.1 | Tropical islands in large-domain RCE simulations

3.1.1 | Distribution of precipitation and deep convection

Figure 1 shows the distribution of mean precipitation occurring during the analysis period of the simulation (days 100–150). The precipitation is organized into

large-scale precipitating and non-precipitating regions, which correspond to large-scale regions of high and low precipitable water. Those regions are akin to the moist and dry regions which have been shown to develop when convection self-aggregates in traditional RCE simulations. In the ensemble mean, the moist region overlaps with the prescribed islands and precipitates on average up to 20 mm·day^{-1}. Offshore, two dry regions form: a first circular region forms to the northwest of Borneo and a second smaller region between the islands of Borneo, Sumatra, and Sulawesi. They precipitate much less than the moist region – on average below 1 mm·day^{-1}.

On the mesoscale, precipitation is additionally shaped by local wind systems that provide dynamical forcing for deep convection initiation. These circulations are well documented in the literature (see Introduction) and emerge from the distinct heat capacity of land and ocean, and from the associated variations in surface heat fluxes (Figure S1). In the presented simulations, a nocturnal land breeze (coastal wind blowing from land to ocean) initiates precipitating deep convection right offshore, leading to a maximum in coastal precipitation around 0800 local time (Figure 2a, b). After sunrise, a sea-breeze forms (coastal wind blowing from ocean to land) which enhances precipitation over land and suppresses it on the seaward side of the coast (Figure 2a, c). Enhancement and suppression vary with island size and layout, and is most pronounced for islands enclosing an area between 100 and 10,000 km^2 (Figure S4). Overall, precipitation over land averages to 7.55, and 4.9 mm·day^{-1} along the coastal ocean (Table 1). The ocean only exhibits about 3 mm of precipitation per day.

TABLE 1 Daily precipitation amount (mm·day^{-1}) over simulation days 100–150

Simulation	Domain mean	Land	Coastal Ocean	Ocean
10LAND	4.20±0.53	7.55±2.32	4.91±0.84	3.1±0.84
5LAND	4.26±0.76	6.32±1.55	4.39±0.46	3.58±0.53

Note: Displayed are the ensemble-mean daily average plus/minus one standard deviation.

During the steady phase of the simulation (days 100–150), the moist region still meanders slowly. When considering instantaneous snapshots from individual ensemble members (rather than the ensemble mean as in Figure 1), the horizontal distribution of deep clouds varies substantially in time, and occasionally the dry regions extend to the islands (Figures 3a, b). That temporal variability in the large-scale moisture field is important, since the diurnal convection initiated by the sea-breeze reliably deepens into precipitating convection only when islands are co-located with the moist region. In the snapshot displayed in Figure 3b, for example, the dry region extends over Borneo while clusters of deep convection are located directly to the west and east. Although on that day diurnal clouds were initiated over the majority of Borneo during the morning hours, they remained shallow in the afternoon (Figure 3c). As a result, diurnal precipitation events do not occur everywhere on land all the time (Table 2) (Section 3.2). More specifically, on land it rains on 51% of the days on average when islands reside under a moist troposphere, and under a dry troposphere it rains on 9% of the days. The ocean receives precipitation only about half as often as land when co-located with a

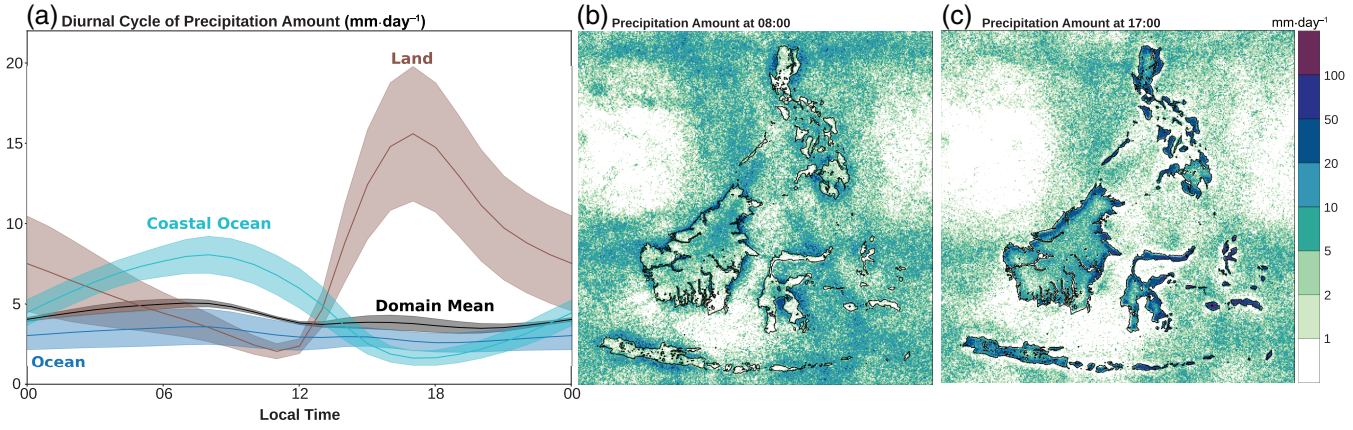

FIGURE 2 Sub-daily precipitation amount in the 10LAND simulation. (a) Diurnal cycle of precipitation over ocean (blue), over the coastal ocean (cyan), over land (brown), and for the domain mean (black). The coloured lines denotes the ensemble mean and the colored shading the standard deviation of the ensemble. (b, c) Ensemble-mean precipitation amount (b) between 0700 and 0800, and (c) between 1600 and 1700 local time. The coloured shading denotes the ensemble-mean precipitation sum, and the black line the island outline [Colour figure can be viewed at wileyonlinelibrary.com]

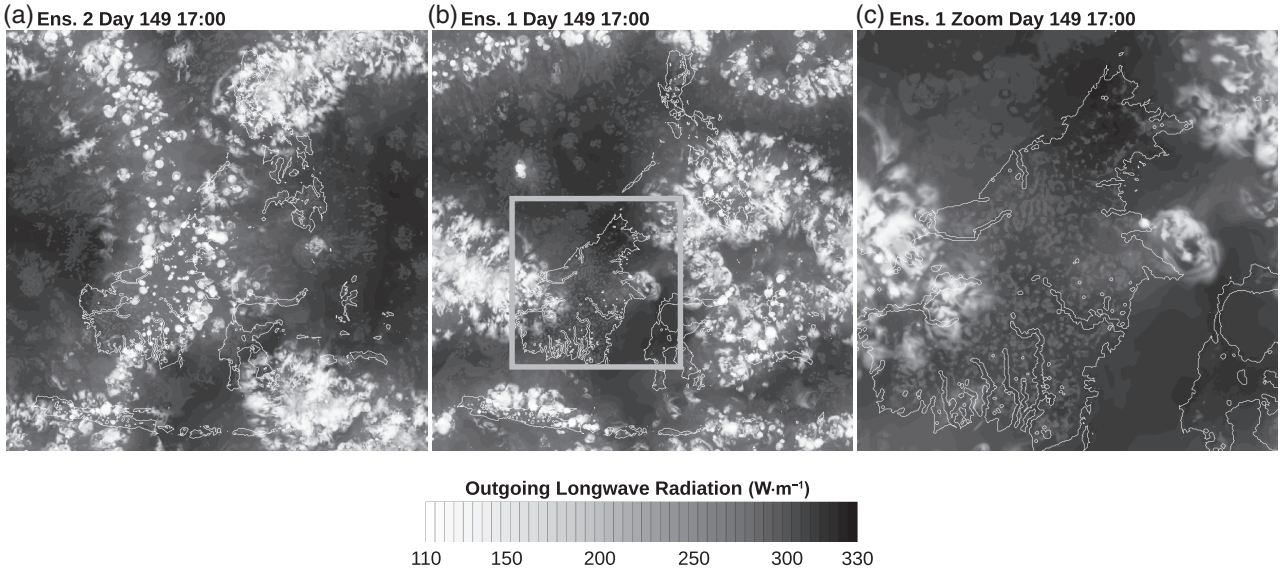

FIGURE 3 Outgoing Long-wave Radiation (OLR, $W \cdot m^{-2}$) obtained from the 10LAND simulation. The white shading indicates OLR and the white lines the island outline. (a, b) Snapshots on day 149 at 1700 local time, taken from ensemble members 2 and 1. (c) Expansion into the grey rectangle in (b)

moist troposphere (24%), and almost never under a dry troposphere (1%).

3.1.2 | Adjustment of tropospheric virtual temperatures to islands

In the absence of rotation, tropospheric horizontal density anomalies are rapidly radiated away by gravity waves. As a consequence, horizontal anomalies in virtual temperature T_v are eliminated at the time-scale set by the wave propagation. Since diurnal precipitation over land is frequent, we expect islands to introduce a detectable signal into the diurnal evolution of mid-tropospheric T_v.

The imprint of the islands on the troposphere can be detected visually in the timing of the ensemble-mean daily T_v maximum on the 560 hPa pressure level (Figure 4). Although the spatial distribution is somewhat chaotic, one can observe several circular wavefronts spreading from the islands (Figure 4a). Near Borneo, for instance, the colour shading becomes successively darker with increasing distance from land, indicative of a propagating wave.

Gravity waves propagate with different speeds and wavelength (Alexander and Holton, 2004). They propagate fastest in the mid-troposphere (black arrow on the 560 hPa pressure level in Figure 4b) with a speed estimated to be about $50\ m \cdot s^{-1}$. This value corresponds to our expectation of a deep first mode gravity wave with a vertical wavelength of 30 km (twice the depth of the heating), as found in other simulations of gravity waves induced by deep heating profiles (e.g., Lane and Reeder, 2001).

Over the islands, a prominent daytime T_v signal can be detected below the 700 hPa pressure level which originates at the shoreline and propagates towards the centre of the islands (at $20\ m \cdot s^{-1}$). At night-time, another signal can be found seaward of the island which propagates to the ocean (at $13\ m \cdot s^{-1}$). The timing of these signals coincides with the formation of clouds, induced by the daytime sea breeze (over land) and the night-time land breeze (over the coastal waters). Note that the night-time sea-breeze signal is affected at its lower edge by the local daytime T_v maximum of the boundary layer, and thus appears awkward.

Spatial averages reveal a systematic propagation on the 560 hPa pressure level (not shown). Over land, the diurnal cycle of T_v attains its maximum at 1500, 2 hr before the peak in diurnal precipitation occurs (at 1700; Figure 2). Over the Coastal Ocean and the Ocean, the T_v maxima occur later in the day (1600 and 1700), more than 8 hr after the diurnal precipitation maxima in these areas, and actually at the time of minimum precipitation over the ocean. The successive timing of the maxima in the three regions (first land, then Coastal Ocean, and ultimately Ocean) suggests adjustment of the domain-mean density, upscaling from the diurnal cycle of precipitation over land.

The analysis presented in Figure 4 suggests that the small fraction of land may influence free-tropospheric temperature by means of density adjustment and subsidence warming. However, does the presence of islands mostly shape when and where convection occurs, or do the islands systematically influence the domain-mean temperature profile? And if so, do they warm, as in Cronin *et al.*

TABLE 2 Ensemble-mean wet-day frequency (%) in the 10LAND and 5LAND simulations, conditioned on the presence of a moist or of a dry troposphere

Simulation	Domain mean	Land	Ocean	Moist Land	Dry Land	Moist Ocean	Dry Ocean
10LAND	15	29	13	51	9	24	1
5LAND	15	24	14	50	7	26	2

Note: The respective wet-day frequency is obtained by first applying a threshold on the daily precipitation sum (P>1 mm·day^{-1}), and then spatially averaging conditioned on the desired (static) land–sea and/or (instantaneous) moist–dry mask. The final wet-day frequency is obtained after taking the temporal average applied over the last 50 simulation days of all ensemble members.

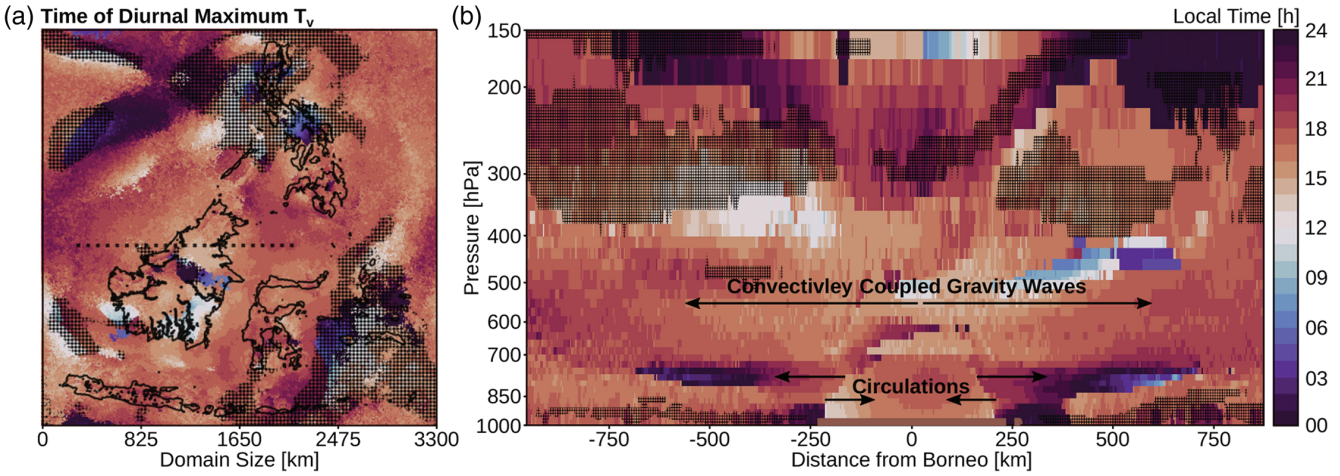

FIGURE 4 Local time of the diurnal maximum in ensemble-mean virtual temperature (T_v) in the 10LAND simulation. The blueish and reddish shadings indicate PM and AM respectively, and the solid black line the island outline. The hatched area marks locations where the amplitude of the diurnal cycle amounts to less than 0.2 K (less than half the domain-mean amplitude). Here the diurnal cycle is often not well defined and, for example, exposes multiple diurnal maxima and minima. (a) Timing at the 560 hPa pressure level, corresponding to the pressure level with the fastest wave propagation detected (uppermost arrow in (b)). The dotted line denotes the location of the cross-section displayed in (b). (b) Cross-section across Borneo. The brown shading at the bottom indicates land. The hand-drawn arrows indicate propagating gravity waves (middle of the panel) and breeze circulations (near the surface). Their length is proportional to the distance a signal travels in 3 hr [Colour figure can be viewed at wileyonlinelibrary.com]

(2015), or do they cool it? In the two subsequent sections, we extend the analysis from diurnal anomalies in virtual temperature to the domain-mean temperature profile. We do so first by assessing how the occurrence of precipitation over land and the mid-tropospheric temperature co-vary, and then by exploiting an additional simulation with reduced land fraction.

3.2 | Modification of bulk mid-tropospheirc temperature by island-based deep convection

To assess the co-variability in the occurrence of precipitation over land and free tropospheric temperature, we examine the variability of precipitation and quantify it by using the wet-land frequency. This metric is defined as the number of land grid points receiving more than 1 mm of precipitation per day divided by the total number of grid points of the computational domain.

During the analysis period, the domain-mean variability of precipitation amount is rather small (Table 1). In other words, time series of precipitation show about the same domain-mean amount each day (now shown). On the other hand, considerable temporal variability can be found in the fraction of land receiving precipitation in the individual ensemble members, as the column water vapour field does not remain static but is meandering slowly (Section 3.1.1). In ensemble member 1, for example, variations in the wet-land fraction of 1% can be observed (brown curve in Figure 5). Episodes exhibiting a higher wet-land fraction correlate with colder domain-mean tropospheric (virtual) temperature (Figure 5). The Pearson correlation coefficient of the first ensemble member (ρ) between wet-land fraction and temperature amounts to about $\rho = -0.91$ in the displayed time series. The corresponding ensemble-mean coefficient amounts to $\overline{\rho} = -0.45$. The anti-correlation between the wet-land fraction and temperature at 500 hPa hints at a colder troposphere when a larger share of precipitation is occurring over land.

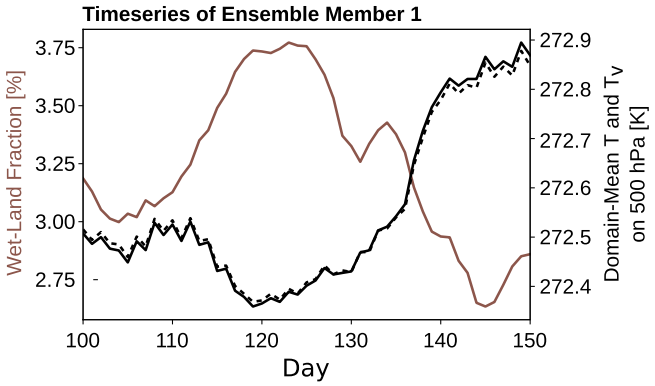

FIGURE 5 Evolution of the wet-land fraction and domain-mean temperature on the 500 hPa pressure level for the last 50 simulation days in ensemble member 1. The brown line denotes the fraction of land receiving more than 1 mm precipitation per day. The solid black line denotes temperature (T) on the 500 hPa pressure level and the dotted black line the virtual temperature (T_v). Note that for visual clarity, a constant of 0.38 K has been subtracted from T_v (domain-mean virtual effect) [Colour figure can be viewed at wileyonlinelibrary.com]

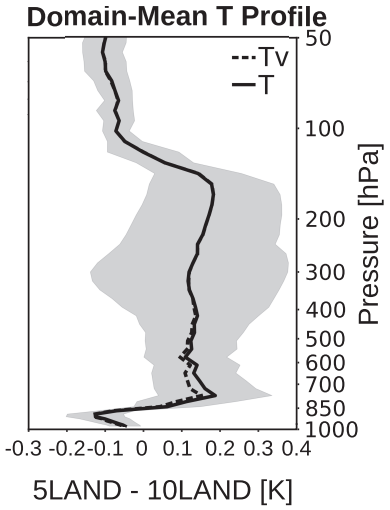

FIGURE 6 Ensemble-mean difference in the domain-mean temperature profiles of the 5LAND and the 10LAND simulation for the days 100–150. The solid (dashed) black line denotes the difference in temperature (virtual temperature). The black shading denotes the standard deviation of the temperature difference obtained when randomly selecting two ensemble members

In other words, the land cools the domain-mean troposphere.

To test this idea further, we supplement another simulation ensemble which has the island of Borneo removed. Based on the results presented so far, we expect the second ensemble to exhibit a warmer free troposphere than the first one, since the land fraction is reduced from 10% (10LAND) to 5% (5LAND).

3.3 | Domain-mean temperature profile in simulations with reduced land fraction

In the 5LAND simulation, the same domain-mean precipitation amount can be found as in 10LAND (Table 1), and rain on an island occurs as frequently when it is located below a moist troposphere (Table 2). A major difference between the two simulations is the large-scale distribution of water vapour, precipitation and clouds. Instead of the meridionally extended moist region overlapping with most of the islands like in 10LAND, here the moist region extends zonally and is only co-located with the Philippines (Section 4). In practice, the fraction of land co-located with a moist troposphere is reduced, and thus the overall wet-day frequency over land is slightly lower in 5LAND (24%) than in 10LAND (29%). In other words, the average wet-land fraction in 5LAND is about 1.2%, while in 10LAND it is about 3%. As a consequence, in 5LAND precipitation amounts are larger over ocean and smaller over land, as compared to 10LAND (Table 1). Nevertheless, the 5LAND simulation still exhibits precipitation enhancement over the islands, but slightly less strong.

The ensemble-mean difference of the domain-mean temperature profiles between 5LAND and 10LAND reveals vertically uniform warming of the free troposphere, a cooling of the sub-cloud layer, and a colder stratosphere when the land fraction is reduced (Figure 6). The signal is interpreted as being significant. First, the domain-mean warming of the free troposphere amounts to about 0.15 K, that is, to about half the amplitude of the domain-mean diurnal cycle at 500 hPa (0.3 K). Second, randomly selecting two ensemble members results in a systematic warming of the free troposphere when the land fraction is reduced (shading in Figure 6). The difference in virtual temperature (T_v) matches that of temperature, indicating that the two simulations yield a similar domain-mean moisture profile. These results are consistent with the analysis presented in Figure 5 and indicate a tendency for the islands to cool the troposphere.

4 | COOLING OF THE FREE TROPOSPHERE

The cooling of the troposphere may be understood by considering the evolution of the sub-cloud layer over land. More specifically, we propose that convection over islands may follow a comparatively colder adiabat than convection over ocean, if relative humidity decreases substantially

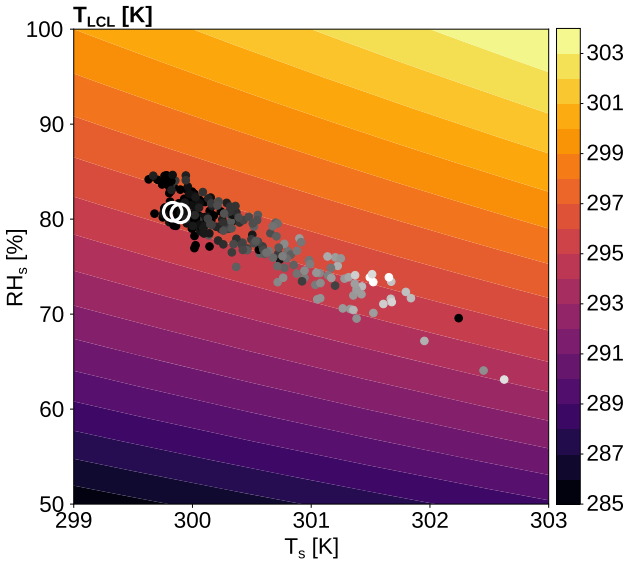

FIGURE 7 Temperature at the lifting condensation level (T_{LCL}, colour shading) estimated from near-surface air temperature (T_s) and relative humidity (RH_s) using the formula proposed by Bolton, (1980). The two white circles denote the diurnal-mean T_{LCL} over ocean, and the filled dots the respective mean T_{LCL} at 1200 local time, for every individual island of 10LAND and 5LAND. The markers are coloured by the island size with lighter colours indicating larger islands. T_s and RH_s were obtained from the lowest model level and spatially averaged to compute the T_{LCL}. Results vary little if T_{LCL} is first computed using an iterative method, and spatially averaged afterwards (Figure S5). All the quantities are computed based on the ensemble-mean estimates in the moist region for the simulation days 100–150 [Colour figure can be viewed at wileyonlinelibrary.com]

enough during the day. The resistance of soils to evaporation leads to an order of magnitude larger daytime Bowen Ratio over land (0.6 at 1200) than over ocean (daily mean value of 0.01), and thus to warmer and less saturated near-surface air over the islands (Figure S3). The daytime hot anomaly over islands leads to convection at a warmer lifting condensation level (LCL), however at the same time, lower relative humidity also elevates the LCL to lower temperatures, as more lifting along the dry adiabat is required until saturation is reached. Deep convection over land may thus end up on a warmer or a colder adiabat compared to ocean, depending on whether the contrasts in near-surface temperature or humidity are more substantial.

The LCL temperature formula by Bolton (1980) confirms that the drying in near-surface relative humidity (RH_s) over islands more than compensates the warming. This can be seen from the steeper slope of the island T_{LCL} estimates in Figure 7, compared to that of the T_{LCL} contours. Also, the contours become less inclined for lower values of RH_s, meaning that, for the dryer islands, even less drying in relative humidity is required to compensate for a surface warming. For example, at RH_s=80% and T_s=300 K (the majority of islands), a 1 K warming in T_s is about compensated by a reduction in RH_s of 4%, while only about 3% is needed at RH_s=60% and T_s=302 K. In other words, the lifting effect over land becomes more pronounced the dryer an island becomes.

The temperature of the LCL over land strongly varies with island size (Figure 7). For small islands, the diurnal minimum T_{LCL} is very similar to the mean over ocean, that is, many black dots in Figure 7 are scattered closely around the white circles. Over these islands, T_{LCL} is about the same as over the ocean, either because RH_s and T_s are similar, or because warming and drying compensate each other. However, once the islands enclose an area of more than 100 km^2 (also Figure S4), the LCL over land becomes slightly colder than over the ocean, and for the

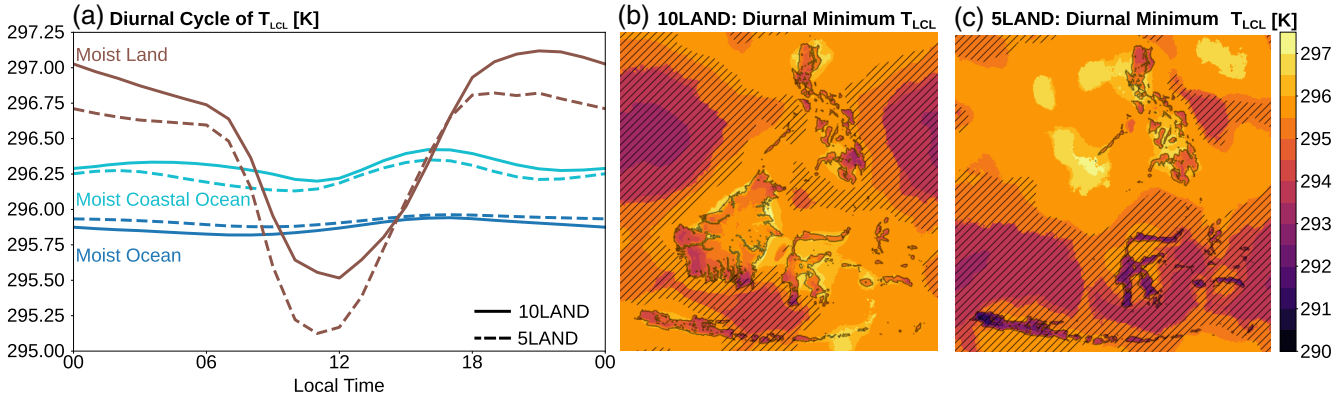

FIGURE 8 Variability of the temperature at the LCL (T_{LCL}). (a) Ensemble-mean diurnal cycle for the 10LAND (full lines) and the 5LAND (dotted) simulations in the moist region. Spatial averages are shown for Land (brown), the Coastal Ocean (cyan) and the Ocean (blue) that coincide with the moist area. (b, c) Diurnal minimum T_{LCL} in the (b) 10LAND and (c) 5LAND simulations. The hatching denotes the (disregarded) dry region [Colour figure can be viewed at wileyonlinelibrary.com]

largest islands T_{LCL} can become more than 2 K colder than over ocean.

The LCL temperature over land exhibits substantial variability in space and time, besides that emerging from island size. For instance, T_{LCL} over land is actually higher than over ocean during night (Figure 8a), but as convection over land is predominantly triggered during the day, the noon and morning values over land are more representative (Figure 2). In addition, T_{LCL} becomes very low during episodes when the land sits under a dry troposphere (Figure 8b, c). That would bias the statistics towards cold values in particular, since during these times, no precipitation tends to occur (Table 2). Therefore, we removed those points from the statistics presented above. Based on these considerations, we conclude that the lower T_{LCL} over land is not a statistical artifact.

5 | CONCLUSIONS

We have conducted a six-member ensemble of idealized RCE simulations using a simulation configuration that includes a set of islands obtained from the Maritime Continent. The imposed diurnal cycle of solar insolation fosters the development of mesoscale coastal breeze circulations that induce afternoon rainfall maxima landside of the coast, and morning maxima seaward. In the afternoon, gravity waves propagate away from the islands over the ocean, connecting the islands to the domain-mean profile by eliminating tropospheric density anomalies originating from diurnal daytime convection.

Similar to RCE simulations without islands, deep convection aggregates into large clusters and organizes the humidity field into large-scale moist and precipitating, as well as dry and non-precipitating, regions. Most of the time, the moist regions align with the islands. During these episodes, substantial island precipitation enhancement can be observed and rainfall is more frequent over land than over the ocean. During episodes when the dry region aligns with the islands, precipitation is overall less frequent, but still more frequent over land than over the ocean. These results portray the well-known effectiveness of the spatial distribution of the large-scale humidity field in shaping precipitation, but they also indicate that it would be misleading to think that convection can never develop in a moderately dry atmosphere. These results are consistent with the findings of Bergemann and Jakob (2016). They have shown that coastal precipitation occurs under a much drier mid-troposphere than over the ocean, and that it does not exhibit a critical humidity threshold.

We found that islands have the potential for modifying the domain-mean tropospheric temperature profile. We observed that temperature on the 500 hPa pressure level becomes warmer during days with less frequent precipitation over land, and colder if precipitation is more frequent. To corroborate this result, we compared two simulation ensembles that have a different land fraction prescribed (10 and 5%). Randomly selecting domain-mean temperature profiles from each of the two simulation ensembles consistently results in a colder free troposphere in the ensemble with more land. These two analyses demonstrate a systematic domain-mean temperature perturbation of less than 1 K related to the presence of land.

A recent hypothesis suggests that the increased variability introduced by surface heterogeneities such as islands will push deep convection towards a warmer moist adiabat, as clouds typically form at the warmest and coincidentally moistest locations of the sub-cloud layer (Cronin *et al.*, 2015). That hypothesis suggests a domain-mean warming of the troposphere by islands, yet our simulations yield a cooling. A modification in our model system explains the observed difference. Instead of representing islands with a local anomaly in the heat capacity of a mixed-layer ocean as in Cronin *et al.* (2015), we employ a land surface scheme that takes into account that, over land, the water supply from the surface is not unlimited, as over ocean. In the absence of precipitation, the soil becomes dry and thus evaporation is limited below its potential rate. As a result, the sub-cloud layer over land not only becomes warmer (surface air temperature) but also dryer (surface relative humidity) than over ocean during the day.

Intuition on these diverging effects can be gained by exploiting the analytic LCL height formula established by Bolton (1980). We propose that the observed domain-mean cooling emerges from the resistance of land to evaporation. While the daytime surface warming yields a warmer LCL, and hence a warmer moist adiabat, the daytime drying elevates the LCL to lower temperatures. Our analysis shows that, for small islands, warming of the LCL is about compensated by the drying, but for large islands, the LCL over land becomes slightly colder than over the ocean. Over large islands, deep convection thus ends up on a weakly colder adiabat than over the ocean. Ultimately, a larger share of convection associated with large islands will thus result in a colder domain-mean troposphere.

The influence of the soil's resistance to evaporation on the LCL height over land has been documented in the literature decades ago (e.g., Betts, 1992). However, soil moisture is only one among many factors controlling the LCL height (e.g., turbulence, island shape, lateral mixing, large-scale flow, topography) over the islands of the Maritime Continent. While these factors warrant

separate assessments, we suggest that the inability of the land to keep up with the daytime surface warming is of key relevance for the temperature profile in the Maritime Continent.

ACKNOWLEDGEMENTS

We would like to thank Julia Windmiller and Jiawei Bao for the their input and the fruitful discussions. The RCE simulations were conducted at the Swiss National Supercomputing Centre CSCS. For the particular version of COSMO, we would like to thank the Federal Office of Meteorology and Climatology MeteoSwiss, the Centre for Climate Systems Modeling (C2SM) and ETH Zurich. In particular, we would like to acknowledge Linda Schlemmer for providing us with an initial set of code modifications for using COSMO in an RCE configuration. COSMO may be used for operational and for research applications by the members of the COSMO consortium. Moreover, within a license agreement, the COSMO model may be used for operational and research applications by other national (hydro-)meteorological services, universities, and research institutes. The particular version of the COSMO model used in this study is based on the official version 5.0 with many additions to enable GPU capability. It is available under a licence (http://www.cosmo-model.org/content/consortium/licencing.htm; accessed 15 February 2021). Primary data and scripts used in the analysis and other supplementary information are archived by the Max Planck Institute for Meteorology and can be obtained at https://hdl.handle.net/21.11116/0000-0007-E293-3. Open access funding enabled and organized by Projekt DEAL.

ORCID

David Leutwyler https://orcid.org/0000-0002-5141-1737
Cathy Hohenegger https://orcid.org/0000-0002-7478-6275

REFERENCES

Alexander, M.J. and Holton, J.R. (2004) On the spectrum of vertically propagating gravity waves generated by a transient heat source. *Atmospheric Chemistry and Physics*, 4, 923–932. https://doi.org/10.5194/acp-4-923-2004.

Arteaga, A., Fuhrer, O. and Hoefler, T. (2014). Designing bit-reproducible portable high-performance applications, pp., 1235–1244 in IEEE 28th International Parallel and Distributed Processing Symposium. Washington DC: IEEE.

Avissar, R. and Liu, Y. (1996) Three-dimensional numerical study of shallow convective clouds and precipitation induced by land surface forcing. *Journal of Geophysical Research: Atmospheres*, 101, 7499–7518.

Baldauf, M., Seifert, A., Förstner, J., Majewski, D., Raschendorfer, M. and Reinhardt, T. (2011) Operational convective-scale numerical weather prediction with the COSMO model: Description and sensitivities. *Monthly Weather Review*, 139, 3887–3905.

Belušić, A., Prtenjak, M.T., Güttler, I., Ban, N., Leutwyler, D. and Schär, C. (2018) Near-surface wind variability over the broader Adriatic region: insights from an ensemble of regional climate models. *Climate Dynamics*, 50, 4455–4480.

Bergemann, M. and Jakob, C. (2016) How important is tropospheric humidity for coastal rainfall in the tropics?. *Geophysical Research Letters*, 43, 5860–5868.

Betts, A.K. (1982) Saturation point analysis of moist convective overturning. *Journal of the Atmospheric Sciences*, 39, 1484–1505.

Betts, A.K. (1992) FIFE atmospheric boundary layer budget methods. *Journal of Geophysical Research: Atmospheres*, 97, 18523–18531.

Beucler, T., Leutwyler, D. and Windmiller, J.M. (2020) Quantifying convective aggregation using the tropical moist margin's length. *Journal of Advances in Modeling Earth Systems*, 12(10). https://doi.org/10.1029/2020MS002092.

Bolton, D. (1980) The computation of equivalent potential temperature. *Monthly Weather Review*, 108, 1046–1053.

Bretherton, C.S., Blossey, P.N. and Khairoutdinov, M. (2005) An energy-balance analysis of deep convective self-aggregation above uniform SST. *Journal of the Atmospheric Sciences*, 62, 4273–4292.

Bretherton, C.S. and Smolarkiewicz, P.K. (1989) Gravity waves, compensating subsidence and detrainment around cumulus clouds. *Journal of the Atmospheric Sciences*, 46, 740–759.

Coppin, D. and Bellon, G. (2019) Physical mechanisms controlling the offshore propagation of convection in the tropics: 1. flat island. *Journal of Advances in Modeling Earth Systems*, 11, 3042–3056.

Cronin, T.W., Emanuel, K.A. and Molnar, P. (2015) Island precipitation enhancement and the diurnal cycle in radiative-convective equilibrium. *Quarterly Journal of the Royal Meteorological Society*, 141, 1017–1034.

Doms, G., Förstner, J., Heise, E., Herzog, H.-J., Mironov, D., Raschendorfer, M., Reinhardt, T., Ritter, B., Schrodin, R., Schulz, J.-P. and Vogel, G. (2011). A description of the nonhydrostatic regional COSMO model. Part II: Physical parameterization. Technical Report LM_F90 4.20. Consortium for Small-Scale Modelling. Available at https://www.cosmo-model.org; accessed 15 February 2021.

Emanuel, K.A., Neelin, D.J. and Bretherton, C.S. (1994) On large-scale circulations in convecting atmospheres. *Quarterly Journal of the Royal Meteorological Society*, 120, 1111–1143.

Fuhrer, O., Osuna, C., Lapillonne, X., Gysi, T., Cumming, B., Arteaga, A. and Schulthess, T.C. (2014) Towards a performance portable, architecture agnostic implementation strategy for weather and climate models. *Supercomputing Frontiers and Innovations*, 1. https://doi.org/10.14529/jsfi140103.

Grabowski, W.W. (2006) Impact of explicit atmosphere–ocean coupling on MJO-like coherent structures in idealized aquaplanet simulations. *Journal of the Atmospheric Sciences*, 63, 2289–2306.

Grabowski, W.W., Yano, J.-I. and Moncrieff, M.W. (2000) Cloud-resolving modeling of tropical circulations driven by large-scale SST gradients. *Journal of the Atmospheric Sciences*, 57, 2022–2040.

Heise, E., Ritter, B. and Schrodin, R. (2006). Operational implementation of the multilayer soil model. Technical Report No. 9. Consortium for Small-Scale Modelling. Available at https://www.cosmo-model.org; accessed 15 February 2021.

Held, I.M., Hemler, R.S. and Ramaswamy, V. (1993) Radiative-convective equilibrium with explicit two-dimensional moist convection. *Journal of the Atmospheric Sciences*, 50, 3909–3927.

Hentgen, L., Ban, N., Kröner, N., Leutwyler, D. and Schär, C. (2019) Clouds in convection-resolving climate simulations over Europe. *Journal of Geophysical Research: Atmospheres*, 124, 3849–3870.

Hohenegger, C. and Stevens, B. (2018) The role of the permanent wilting point in controlling the spatial distribution of precipitation. *Proceedings of the National Academy of Sciences of the USA*, 115, 5692–5697.

Houze, R.A., Geotis, S.G., Marks, F.D. and West, A.K. (1981) Winter monsoon convection in the vicinity of North Borneo. Part I: structure and time variation of the clouds and precipitation. *Monthly Weather Review*, 109, 1595–1614.

Klemp, J.B., Dudhia, J. and Hassiotis, A.D. (2008) An upper gravity-wave absorbing layer for NWP applications. *Monthly Weather Review*, 136, 3987–4004.

Lane, T.P. and Reeder, M.J. (2001) Convectively generated gravity waves and their effect on the cloud environment. *Journal of the Atmospheric Sciences*, 58, 2427–2440.

Leutwyler, D., Fuhrer, O., Lapillonne, X., Lüthi, D. and Schär, C. (2016) Towards European-scale convection-resolving climate simulations with GPUs: a study with COSMO 4.19. *Geoscientific Model Development*, 9, 3393âĂŞ3412. https://doi.org/10.5194/gmd-9-3393-2016.

Leutwyler, D., Lüthi, D., Ban, N., Fuhrer, O. and Schär, C. (2018) Evaluation of the convection-resolving climate modeling approach on continental scales. *Journal of Geophysical Research: Atmospheres*, 122, 5237–5258.

Love, B.S., Matthews, A.J. and Lister, G.M.S. (2011) The diurnal cycle of precipitation over the Maritime Continent in a high-resolution atmospheric model. *Quarterly Journal of the Royal Meteorological Society*, 137, 934–947.

Mapes, B.E. and Houze, R.A. (1993) Cloud clusters and superclusters over the oceanic warm pool. *Monthly Weather Review*, 121, 1398–1416.

Mellor, G. and Yamada, T. (1982) Development of a turbulence closure model for geophysical fluid problems. *Reviews of Geophysics*, 20, 851–875.

Mori, S., Jun-Ichi, H., Tauhid, Y.I., Yamanaka, M.D., Okamoto, N., Murata, F., Sakurai, N., Hashiguchi, H. and Sribimawati, T. (2004) Diurnal land–sea rainfall peak migration over Sumatera Island, Indonesian Maritime Continent, observed by TRMM satellite and intensive rawinsonde soundings. *Monthly Weather Review*, 132, 2021–2039.

Owens, J., Houston, M., Luebke, D., Green, S., Stone, J. and Phillips, J. (2008) GPU computing. *Proceedings of the IEEE*, 96, 879–899.

Qian, J.-H. (2008) Why precipitation is mostly concentrated over islands in the Maritime Continent. *Journal of the Atmospheric Sciences*, 65, 1428–1441.

Raschendorfer, M. (2001) The new turbulence parameterization of LM. *COSMO Newsletter*, 1, 89–97. http://www.cosmo-model.org/; accessed 15 February 2021.

Reinhardt, T. and Seifert, A. (2005) A three-category ice-scheme for LMK. *COSMO Newsletter*, 6, 115–120. http://www.cosmo-model.org/; accessed 15 February 2021.

Ritter, B. and Geleyn, J.F. (1992) A comprehensive radiation scheme for numerical weather prediction models with potential applications in climate simulations. *Monthly Weather Review*, 120, 303–325.

Robinson, F.J., Sherwood, S.C. and Li, Y. (2008) Resonant response of deep convection to surface hot spots. *Journal of the Atmospheric Sciences*, 65, 276–286.

Ruppert, J.H. and Chen, X. (2020) Island rainfall enhancement in the Maritime Continent. *Geophysical Research Letters*, 47(5). https://doi.org/10.1029/2019GL086545.

Ruppert, J.H. and Hohenegger, C. (2018) Diurnal circulation adjustment and organized deep convection. *Journal of Climate*, 31, 4899–4916.

Ruppert, J.H. and Zhang, F. (2019) Diurnal forcing and phase locking of gravity waves in the Maritime Continent. *Journal of the Atmospheric Sciences*, 76, 2815–2835.

Schär, C., Fuhrer, O., Arteaga, A., Ban, N., Charpilloz, C., Di Girolamo, S., Hentgen, L., Hoefler, T., Lapillonne, X., Leutwyler, D., Osterried, K., Panosetti, D., Rüdisühli, S., Schlemmer, L., Schulthess, T., Sprenger, M., Ubbiali, S. and Wernli, H. (2020) Kilometer-scale climate models: prospects and challenges. *Bulletin of the American Meteorological Society*, 101, E567–E587. https://doi.org/10.1175/BAMS-D-18-0167.1.

Schlemmer, L., Hohenegger, C., Schmidli, J., Bretherton, C.S. and Schär, C. (2011) An idealized cloud-resolving framework for the study of midlatitude diurnal convection over land. *Journal of the Atmospheric Sciences*, 68, 1041–1057.

Segal, M. and Arritt, R. (1992) Nonclassical mesoscale circulations caused by surface sensible heat-flux gradients. *Bulletin of the American Meteorological Society*, 73, 1593–1604.

Shamekh, S., Muller, C., Duvel, J.-P. and D'Andrea, F. (2020) How do ocean warm anomalies favor the aggregation of deep convective clouds?. *Journal of the Atmospheric Sciences*, 77, 3733–3745. https://doi.org/10.1175/JAS-D-18-0369.1.

Sobel, A.H., Burleyson, C.D. and Yuter, S.E. (2011) Rain on small tropical islands. *Journal of Geophysical Research: Atmospheres*, 116(D8). https://doi.org/10.1029/2010JD014695.

Sobel, A.H., Nilsson, J. and Polvani, L.M. (2001) The weak temperature gradient approximation and balanced tropical moisture waves. *Journal of the Atmospheric Sciences*, 58, 3650–3665.

Steppeler, J., Doms, G., Schättler, U., Bitzer, H.W., Gassmann, A., Damrath, U. and Gregoric, G. (2003) Meso-gamma scale forecasts using the nonhydrostatic model LM. *Meteorology and Atmospheric Physics*, 82, 75–96.

Tompkins, A.M. (2001) Organization of tropical convection in low vertical wind shears: The role of water vapor. *Journal of the Atmospheric Sciences*, 58, 529–545.

Tompkins, A.M. and Craig, G.C. (1998) Radiative-convective equilibrium in a three-dimensional cloud-ensemble model. *Quarterly Journal of the Royal Meteorological Society*, 124, 2073–2097.

Ulrich, M. and Bellon, G. (2019) Superenhancement of precipitation at the center of tropical islands. *Geophysical Research Letters*, 46, 14872–14880.

Wang, S. and Sobel, A.H. (2017) Factors controlling rain on small tropical islands: diurnal cycle, large-scale wind speed, and topography. *Journal of the Atmospheric Sciences*, 74, 3515–3532.

Wicker, L. and Skamarock, W. (2002) Time-splitting methods for elastic models using forward time schemes. *Monthly Weather Review*, 130, 2088–2097.

Wing, A.A., Emanuel, K., Holloway, C.E. and Muller, C. (2017). Convective self-aggregation in numerical simulations: a review. In R.

Pincus, D. Winker, S. Bony, and B. Stevens (Eds.), *Shallow Clouds, Water Vapor, Circulation, and Climate Sensitivity*, pp. 1–25. Berlin: Springer.

Wing, A.A., Reed, K.A., Satoh, M., Stevens, B., Bony, S. and Ohno, T. (2018) Radiative–convective equilibrium model intercomparison project. *Geoscientific Model Development*, 11, 793–813. https://doi.org/10.5194/gmd-11-793-2018.

Xu, K.-M. and Emanuel, K.A. (1989) Is the tropical atmosphere conditionally unstable?. *Monthly Weather Review*, 117, 1471–1479.

Yamanaka, M.D., Ogino, S.-Y., Wu, P.-M., Jun-Ichi, H., Mori, S., Matsumoto, J. and Syamsudin, F. (2018) Maritime Continent coastlines controlling Earth's climate. *Progress in Earth and Planetary Science*, 5(21). https://doi.org/10.1186/s40645-018-0174-9.

Yang, D. (2018) Boundary-layer diabatic processes, the virtual effect, and convective self-aggregation. *Journal of Advances in Modeling Earth Systems*, 10, 2163–2176.

Yang, G.-Y. and Slingo, J.M. (2001) The diurnal cycle in the tropics. *Monthly Weather Review*, 129, 784–801.

SUPPORTING INFORMATION

Additional supporting information may be found online in the Supporting Information section at the end of this article.

How to cite this article: Leutwyler D, Hohenegger C. Weak cooling of the troposphere by tropical islands in simulations of the radiative-convective equilibrium. *Q.J.R. Meteorol. Soc.*. 2021;147:1788–1800. https://doi.org/10.1002/qj.3995